AIAA JOURNAL
Vol. , No. ,

Repetitive Energy Deposition at a Supersonic Intake in Subcritical and Buzz Modes

Manabu Myokan,* Akiya Kubota,* Akira Iwakawa,† and Akihiro Sasoh‡
Nagoya University, Nagoya 464-8601, Japan

https://doi.org/10.2514/1.J058519

This study experimentally investigated the effects of repetitive laser energy deposition using a supersonic intake model with a central conical compression surface and a 19×19 mm^2 cross-sectional duct in a Mach 1.92 indraft wind tunnel: especially in the subcritical and buzz modes. A single-pulse energy deposition was observed to suppress the flow separation at the compression surface by "sweeping" a shock wave system with the thermal bubble generated by the energy deposition. The duration of the sweeping effect was approximately 160 μs in the subcritical mode and 100–420 μs in the buzz mode. Furthermore, repetitive deposition of laser pulse energies was observed to moderate instabilities in both modes, and it increased the pressure recovery by as much as 8%; also, the occurrence of buzz was delayed, thereby widening the stable, subcritical regime. In both modes, there was a threshold value for the laser pulse repetition frequency $f_{L,\mathrm{thd}}$, which corresponded to the duration of the sweeping effect (e.g., $f_{\mathrm{thd}} = 6$ kHz in subcritical mode). Below this frequency, the increase in the pressure was proportional to the repetition frequency; whereas above f_{thd}, the effect per single pulse was reduced.

Nomenclature

A_e	=	flow passage area at the exit, mm^2
A_t	=	flow passage area in the cylindrical section of centerbody, mm^2
A_∞	=	flow passage area at the front rectangular cowl without centerbody, mm^2
a	=	speed of sound
$\hat{c}_d$	=	speed of sound in the duct; characteristic value, m/s
D	=	diameter of the centerbody, mm
f	=	frequency of the flow oscillation, kHz
$f_{B,n}$	=	nth mode frequency of buzz, kHz
f_L	=	frequency of laser energy deposition, kHz
$f_{L,\mathrm{thd}}$	=	threshold frequency of f_L, kHz
L_c	=	extrusion length of the centerbody from the inlet of the square duct, mm
L_d	=	total length of the duct, mm
M_d	=	averaged flow Mach number in the duct
n	=	integer equal or larger than 0
p	=	static pressure
$\bar{p}_{\mathrm{pitot}}$	=	time-averaged pitot pressure measured in the duct, kPa
$\bar{p}_{\mathrm{st}}$	=	time-averaged static pressure measured in the duct, kPa
$\bar{p}_{\mathrm{total},\infty}$	=	time-averaged total pressure in the upstream flow, kPa
t	=	time, μs
α_c	=	A_∞/A_t
α_e	=	A_e/A_t
δ	=	standoff distance of cowl shock, mm
ρ	=	density, kg/m^3

I. Introduction

A SUPERSONIC intake is an important component in a supersonic aircraft propulsion system. Its main function is to compress and decelerate the incoming supersonic flow to a subsonic speed, ensuring a minimal entropy/pressure loss in the associated compression processes. However, intake performance is significantly degraded when there is a significant shock-wave/boundary-layer interaction (SWBLI) [1], which is caused by an adverse pressure gradient along the boundary layer generated behind a shock wave. Once strong interaction appears in a supersonic intake, the performance of the intake is seriously deteriorated due to internal flow separation, decrease in pressure recovery, and shock wave oscillation called buzz, finally leading to its unstart. Therefore, to improve the supersonic intake performance, SWBLI control is important.

The most common method of SWBLI control in the supersonic intake is boundary-layer bleeding [2]. Trapier et al. [3] investigated the effect of bleeding at three different Mach numbers; they reported improvement in the intake performance, and they moderated the pressure fluctuation in the buzz mode. Soltani et al. [4] parametrically examined the effects of upstream bleeding, and they reported improvement in the intake performance and delaying the occurrence of buzz. However, although bleeding is an established and effective scheme, it is accompanied by a mass loss and complication of the mechanical structure. Therefore, further investigation is required to develop more advanced methodologies for SWBLI control [5].

Since the beginning of the 2000s, the "energy deposition" (ED) [6] scheme has been studied to control both external and internal supersonic flows. In ED, high-speed flows (particularly, supersonic flows) are moderated by deposition energy using a laser pulse or electrical discharge such that a low-density/high-temperature region is generated to interact with the shock waves and associated flows. Leonov et al. [7] and Falepin et al. [8] conducted experiments on flow control using plasma in a supersonic inlet and confirmed the modulation of the flowfield. Narayanaswamy et al. [9,10] intermittently deposited energies by plasma jets over an SWBLI region in the supersonic ramp flow and suppressed SWBLI-oriented flow instability. Osuka et al. [11] investigated the effect of repetitive laser energy depositions on a SWBLI over a hemisphere–cylinder–flare model in a Mach 2 flow, and they demonstrated the suppression of flow separation and shock wave oscillation caused by the SWBLI. They attributed such an effect to the behavior of a thermal bubble, which is a low-density/high-temperature region generated by the laser-induced breakdown. Pham et al. [12] investigated the effects on the supersonic flow over a double cone using the same scheme and confirmed the suppression of the separation and the flow instability occurring on the double-cone surface. Furthermore, Pham et al. [13] investigated the energy deposition effect on an axisymmetric supersonic intake model and confirmed the suppression of the flow separation at the compression surface and shock wave oscillation in the pulsation mode near the critical operation regime, thereby

Presented as Paper 2019-2870 at the AIAA 2019 AIAA Aviation Forum, Dallas, Texas, 17–21 June 2019; received 28 March 2019; revision received 12 July 2019; accepted for publication 21 September 2019; published online XX epubMonth XXXX.

*Graduate Student, Department of Aerospace Engineering.
†Lecturer, Department of Aerospace Engineering. Member AIAA.
‡Professor, Department of Aerospace Engineering. Associate Fellow AIAA.

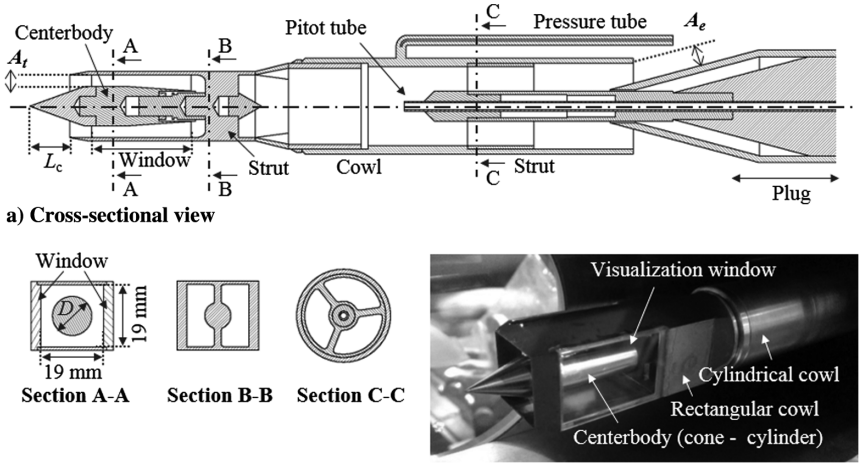

Fig. 1 Schematics and photograph of the intake model.

increasing the pressure recovery. Laser energy deposition is considered to be capable of realizing a nonintrusive flow control, and the current state-of-the-art fiber laser system can output even to 100 kW with an energy conversion efficiency on the order of 40% or higher. As its resonator (i.e., the optical fibers) is lightweight and the associated technique is rapidly advancing, this technology is expected to be practically available with reasonable efficiency and weight in the near future.

Depending on the flow rate, the supersonic intake operation is subdivided to four modes [3,4]. In the supercritical mode, the shock system at the entrance of the intake is not affected by the flow at the exit: in this mode, the flow rate is the highest. The incoming flow is not decelerated much before it is suddenly decelerated by a strong shock wave, which is accompanied by a significant pressure loss. In the critical mode, the exit condition affects the flow condition at the entrance, leading to a decrease in the flow rate. In the subcritical mode, the pressure loss due to compression decreases with decreasing flow rate. However, when the flow passage area becomes too small, the total pressure decreases because of the increase in the flow spillage at the entrance. In the buzz mode, a strong shock wave stands and oscillates at the entrance, thereby exhibiting unstable and degraded intake performance. Therefore, the effects of repetitive energy deposition in the subcritical and buzz modes are more important in the practical intake operation. However, to the best of the authors' knowledge, these have not been sufficiently investigated. Particularly in the buzz mode, the flow fluctuation caused by shock wave oscillation leads to serious destabilization of the engine operation.

The fundamental mechanisms of buzz were first studied by Ferri and Nucci [14] and Dailey [15]. Fisher et al. [16] categorized buzz into two types with respect to the oscillation amplitude and trigger mechanisms. A "Ferri-type" buzz appears when the mass flow rate at the intake begins to decrease from the design point, which is caused by the shear flow near the cowl. On the other hand, a "Dailey-type" buzz, which appears when the mass flow rate decreases further, is caused by the separation of the flow due to SWBLI in the compression section. Lee et al. [17] investigated the buzz phenomenon in a small supersonic intake model from experiments and calculations, and they extensively summarized two types of buzz that appeared due to flow rate changes. Applying the results of the past studies, which demonstrate the effectiveness of energy deposition for SWBLI, it is expected that the Dailey-type buzz caused by a SWBLI can also be suppressed by energy deposition. Therefore, in this study, we aim to systematically investigate the effect of repetitive laser energy deposition on a Mach 1.92 intake operation, particularly in the subcritical and buzz modes, where large pressure recovery is expected and desired.

II. Apparatus and Methods

The study was conducted in an indraft supersonic wind tunnel with an effective flow Mach number of 1.92 ± 0.04 [11–13,18–20]. The

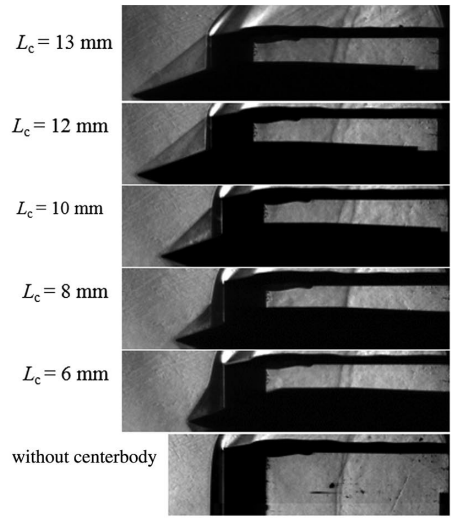

Fig. 2 Effect of L_c on flowfield and internal pressures at D = 11 mm and α_e = 1.62.

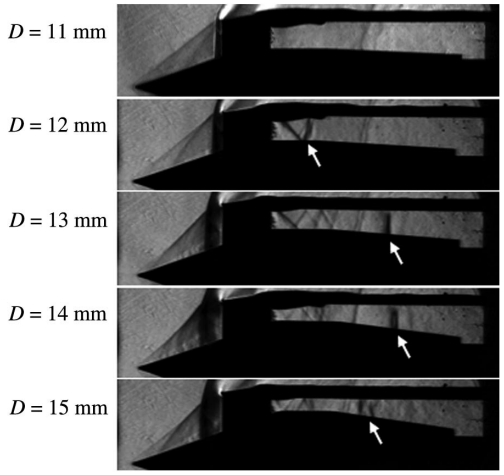

Fig. 3 Schlieren images for different D at $L_c = 12$ mm and $\alpha_e = 1.62$. The arrow indicates the position of terminal shock.

facility allows for a maximum runtime of ~30 s. The cross section of the test section was 80×80 mm^2 fitted with a pair of BK7 windows for flow visualization and laser pulse transmission. The Nd:YVO4 laser (EdgeWave, InnoSlab laser HD40I-E, with wavelength of 1064 nm, maximum power up to 400 W, and maximum repetition frequency of 100 kHz) was used as a source of laser pulse energy to generate a thermal bubble. The shape of the output laser beam was a 6×6 mm^2, which was expanded to 16×16 mm using a beam expander composed of a concave lens and planoconvex lens. After being reflected by two mirrors, the beam was focused in front of a test model through the borosilicate crown (BK7) window on the wind-tunnel wall by a GRADIUM® lens with a focal length of 60 mm. For flow visualization, a high-speed camera (Vision Research, Inc., Phantom v1211, with a maximum resolution of 1280×800 pixels, a maximum speed of 8.2×10^5 frames per second, and a duration of up to 2048 monochromatic 8 bit frames) and a laser light source (Cavitar, Ltd., CAVILUX Smart, with a wavelength of 640 nm, and a pulse duration of 10 ns) were used. The measurement data were recorded on

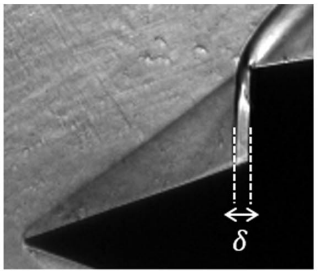

a) Definition of δ at α_e=1.62

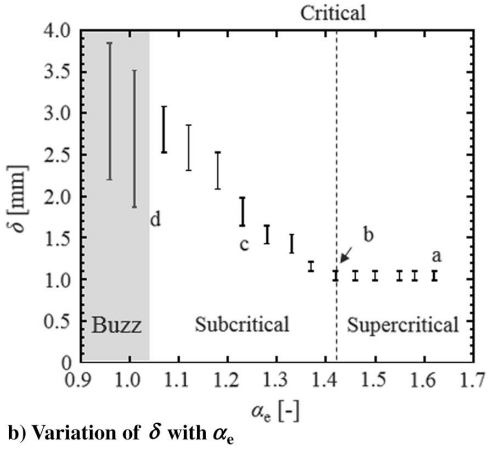

b) Variation of δ with α_e

Fig. 4 Definition of intake operating modes.

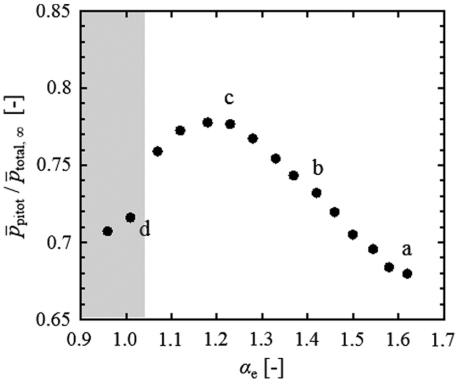

Fig. 5 Variation of pressure recovery with α_e.

a digital oscilloscope (Yokogawa Test and Measurement Corporation, DL750, with a maximum sampling rate of 10 MS/s).

As the next stage to the previous study [13], a new, supersonic intake model with a central compression body composed of a single cone–cylinder body and a rectangle cowl fitted with a BK7 windows were manufactured. A schematic illustration and photograph of the test model are displayed in Fig. 1. The BK7 windows were attached to both sides of the rectangular cowl, as shown in Fig. 1b; the internal flow of the model was visualized through these. There is a smooth transition from the square cross section at the front to a circular cross section at the rear: the cross-sectional area of the front rectangular cowl is 19×19 mm. The total length of the cowl L_d was 170 mm, and the half-apex angle of the single cone was set to 20 deg. The effects of L_c and D of the centerbody were experimentally examined for optimal values. Furthermore, to study the effect of energy deposition on different intake operating conditions, a back plug was installed at the exit of the intake system. This plug could be moved forward and backward by a screw mechanism to control the flow passage area at the exit. The position of the back plug is denoted by α_e (see Fig. 1a).

A high-speed framing schlieren visualization was conducted at a framing rate ranging from 15,362 to 120,300 frames per second. A bandpass filter (Asahi Spectra, Inc., PB0640-020) at a wavelength of 641.5 nm and a width at a half-maximum of 15 nm was set in front of the camera to eliminate luminescence induced by the optical breakdown. The grayscale schlieren image was analyzed using fast Fourier transform (FFT) [12,13,19,20]. The frequency resolution of

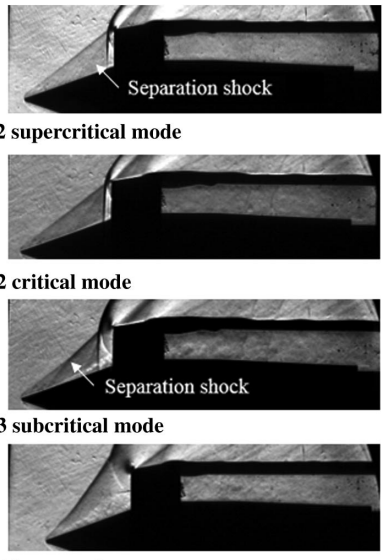

a) α_e = 1.62 supercritical mode

b) α_e = 1.42 critical mode

c) α_e = 1.23 subcritical mode

d) α_e = 1.01 buzz mode

Fig. 6 Schlieren images at four different operating modes. The video file of Fig. 6d is available as Supplemental Video S1.

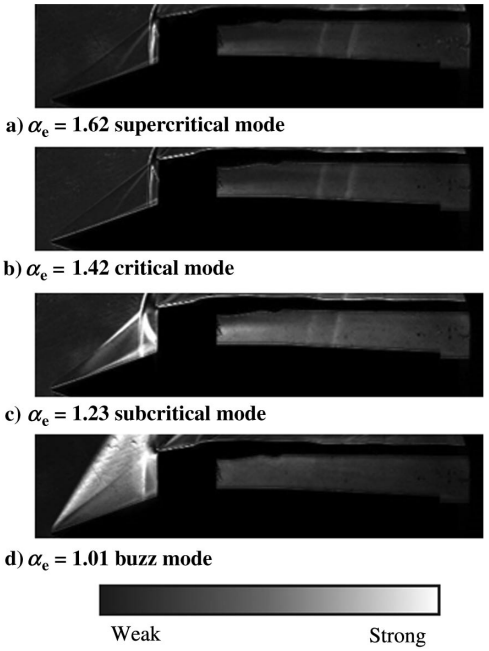

Fig. 7 SD images at four different operating modes.

the FFT was 0.06 kHz, and the maximum frequency depended on the framing rate.

A pitot tube connected to a pressure transducer (Tokyo Aircraft Instrument Company, Ltd., digital pressure gauge DG-921A) was used to measure the time-averaged value of the total pressure inside the intake model $\bar{p}_{\text{pitot}}$ (see Fig. 1a). The time-averaged value of the static pressure on the inner wall $\bar{p}_{\text{st}}$ was also measured using another combination. The response frequency of the transducer was 1 kHz. The pressure signal was averaged in 0.3 s with and without laser energy deposition. When measuring the fluctuation in the pitot pressure, the pitot tube was replaced by a piezoelectric pressure transducer (H112A21, PCB, Inc., with a rise time of 1 μs, and a sensitivity of 7.391 mV/kPa). The sampling rate in the pressure measurement was 500 kHz or 1 MHz, the maximum frequency of the FFT was 250 or 500 kHz, and the frequency resolution was 3.8 Hz.

III. Experimental Conditions and Control Parameters

The followings were the conditions used for the test flow: Mach number of 1.92 ± 0.04; static pressure of 13.8 kPa; static temperature of 170 K, which was estimated by assuming an isentropic flow; and air density of 0.30 kg/m^3. The duration of each wind-tunnel run was approximately 4 s. The geometrical parameters of the intake model were varied in the following ranges: L_c from 6 to 13 mm, and D from 11 to 15 mm. The contraction ratio α_c (see Fig. 1a) was changed from 0.51 to 0.74, and α_e was changed from 0.96 to 1.62. The Reynolds number R_e (which was based on a wind-tunnel flow speed of 480 m/s, the length of one side of the rectangular duct of 19 mm, the static temperature of 163 K, and the density of 0.30 kg/m^3) was equal to 3×10^5. The laser pulse energy was set to a constant value of 5.3 ± 0.3 mJ/pulse, and f_L was varied up to 50 kHz.

IV. Supersonic Intake Flow Without Energy Deposition

A. Effects of L_c

Figure 2 displays the effect of L_c on the intake flow, $\bar{p}_{\text{pitot}}$, and $\bar{p}_{\text{st}}$. In the flow with $L_c = 12$ mm (Fig. 2a), the leading, conical shock generated from the cone tip was best matched with the cowl lip position, and the pressure was maximum. At $L_c < 10$ mm, the leading conical shock did not cover the entire inlet area; the entropy

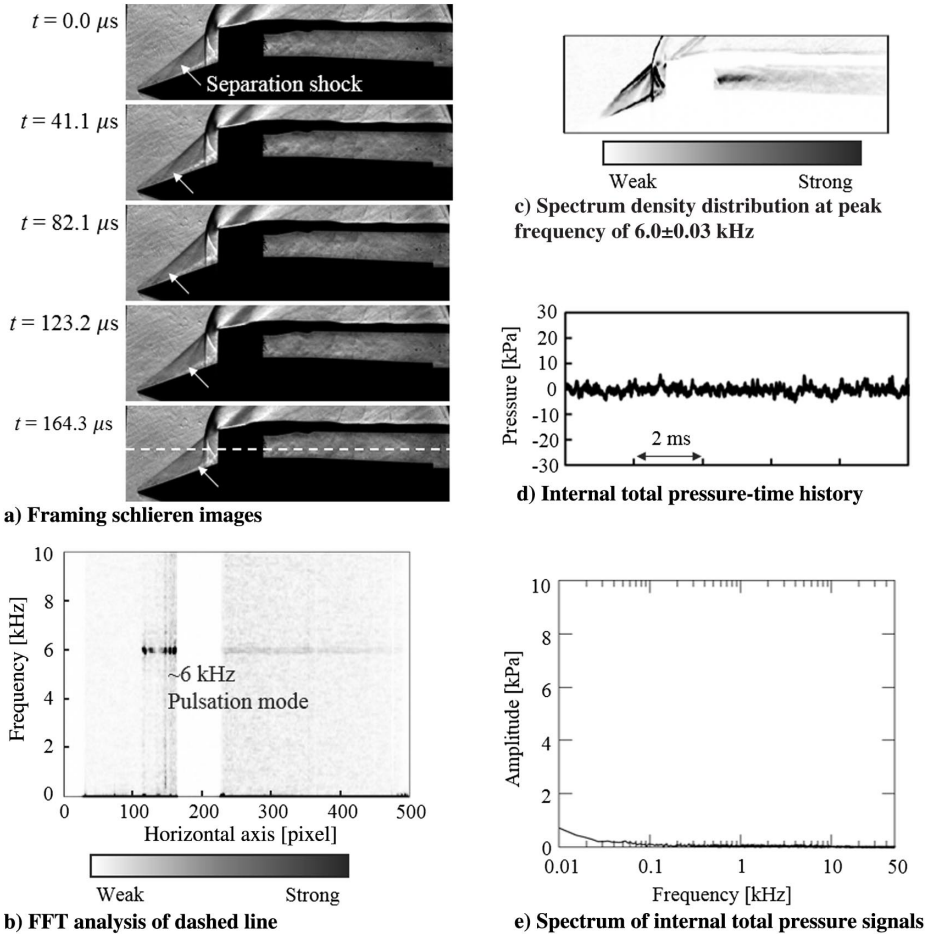

Fig. 8 Flow characteristics at $\alpha_e = 1.23$: subcritical mode.

loss due to the cowl shock increased. Consequently, $\bar{p}_{\text{pitot}}$ and $\bar{p}_{\text{st}}$ decreased with decreasing L_c. Without the centerbody, the intake operation would be unstarted, and hence the pressure is minimum. If $L_c > 12$ mm, the internal pressure decreases due to flow spillage. Therefore, in the following experiments, L_c was set to 12 mm to obtain the maximum pressure recovery.

B. Effects of D

Figure 3 displays the schlieren images for different values of D and at the largest value of $\alpha_e = 1.62$. When $D = 11$ mm, the shock wave reflection is not visualized in the internal flow; the incoming flow appears to be compressed without any significant loss because the oblique shock wave from the cone just reaches the cowl entrance; therefore, there is no reflection of the oblique shock wave on the cowl wall. However, when $D = 12$ mm or greater, a shock system appears in the internal flow; the oblique shock waves repeat the reflections between the cowl wall and the centerbody up to a terminal shock, which is a normal shock wave that decelerates the flow to subsonic speed. With increasing D, the flow passage area between the centerbody and the cowl inner wall decreases, thereby strengthening the SWBLI on the compression surface of the centerbody. When $D = 12$ mm, the oscillation of the separation shock wave is observed; and when $D = 13$ mm or more, the incoming flow to the intake including the conical shock generated from the cone tip oscillates significantly, enhancing the flow spillage. Furthermore, for $D = 12$ to 14 mm, the position of the terminal shock (i.e., the shock wave position beyond which the flow changes from supersonic to subsonic) moves downstream and slightly oscillates. In the following experiments, D was set to a constant value of 11 mm to allow the incoming flow to be compressed most efficiently and stably.

C. Operation Modes with Varying Values of α_e

Typically, the operating condition of an intake is characterized by the relation between the mass flow rate and internal pressure. However, in the present intake model, the mass flow rate could not be measured directly. Rather, the standoff distance of the shock wave in front of the cowl lip (hereafter referred to as "cowl shock") in the schlieren image δ (see Fig. 4a) was used to represent the mass flow rate characteristics. When the cowl shock moves upstream, the mass flow spillage increases, and the incoming mass flow decreases. Therefore, the incoming mass flow rate should monotonically decrease with increasing δ. The schlieren image in Fig. 4a corresponds to the flow with a maximum value α_e. However, the cowl shock is detached because, owing to practical manufacturing limits, the thickness of the cowl lip did not vanish. Figure 4b displays the relationship between the experimentally measured values of δ and α_e. The spatial resolution of the schlieren image was 0.11 mm/pixel; the length of a vertical bar in Fig. 4b corresponds to the oscillation amplitude of the cowl shock location. As α_e decreases from 1.62, δ remains constant until $\alpha_e = 1.42$, and then it increases. This indicates that the incoming mass flow was constant from $\alpha_e = 1.62$ to 1.42, and it decreased below $\alpha_e = 1.42$. Based on the definition of operating mode in Ref. [3], the operation at $\alpha_e = 1.62$ to 1.42 corresponds to the "supercritical mode"; similarly, $\alpha_e = 1.42$ corresponds to the "critical mode", below which is the "subcritical mode." Moreover, at $\alpha_e = 1.01$ and less, a large-scale oscillation of the leading shock wave over the compression surface was observed (i.e., "buzz" mode).

Figure 5 represents the variation of the measured pressure recovery with α_e, which shows that, in the supercritical mode, the pressure recovery increases as α_e decreases. The pitot pressure is determined by the flow modulation past the shock system, which indicates that,

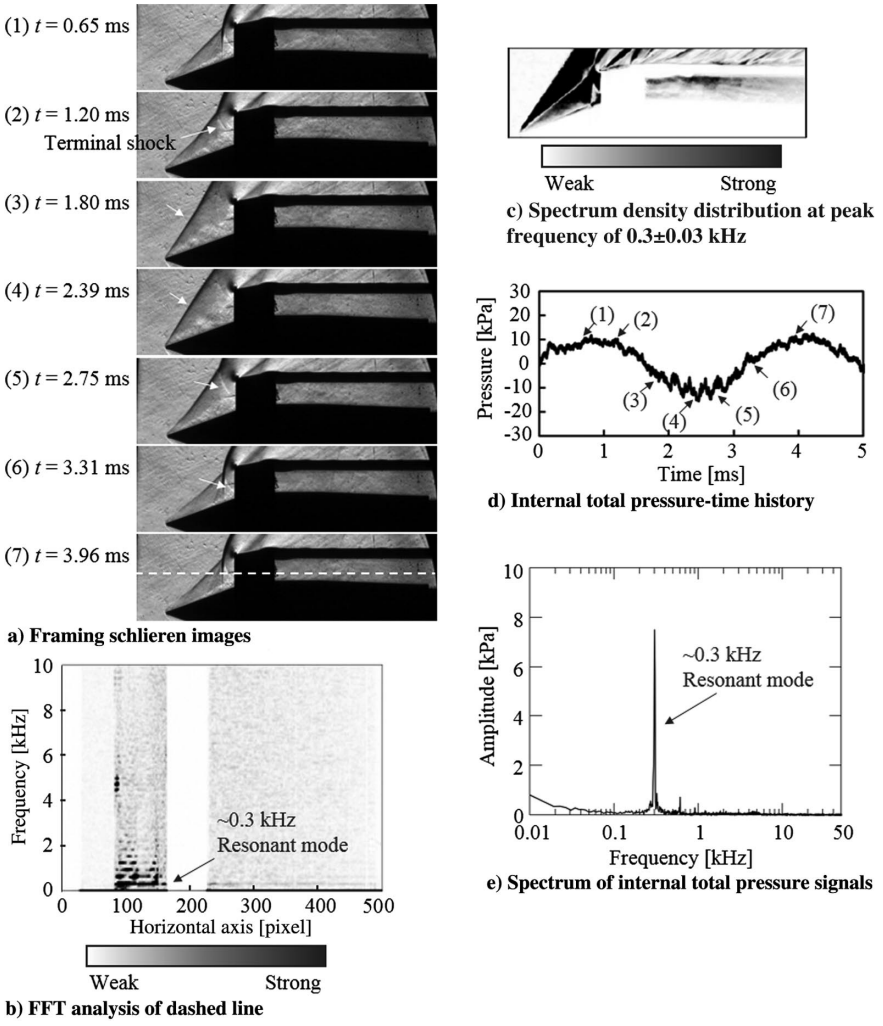

Fig. 9 Flow characteristics at $\alpha_e = 1.01$ buzz mode.

even if the cowl shock is strong, the flow in the downstream of the terminal shock remains supersonic. The total pressure becomes high because a terminal shock is weak. On the other hand, if the cowl shock is weak, the flow Mach number behind the cowl shock remains high, leading to a larger pressure loss behind the terminal shock. With decreasing A_e, and thereby α_e, the ratio of the flow passage area at the pitot probe to that at the exit increases. As the flow is choked with a constant static pressure at the exit, this increment in the ratio leads to an increase in the static pressure at the pitot probe, which should be matched with a larger pressure recovery past the shock system. However, if α_e is too small, the effect of the flow spillage dominates; therefore, the pitot pressure decreases with decreasing α_e. The highest value of pitot pressure is achieved at $\alpha_e = 1.18$ in the subcritical mode. Decreasing α_e further decreases the pressure recovery. In the buzz mode at $\alpha_e = 1.01$ or less, the pressure recovery is observed to decrease sharply.

Figure 6 displays the schlieren images in different operating modes. The distribution of the standard deviation (SD) in the grayscale schlieren images was obtained from approximately 1000 frames recorded for approximately 10 ms in each case, as displayed in Fig. 7. Figures 6a and 7a to Figs. 6d and 7d correspond to points a–d indicated in Figs. 4b and 5. In the supercritical (Figs. 6a and 7a) and critical (Figs. 6b and 7b) modes, the SWBLI induced a flow separation, which in turn induced a separation shock wave; yet, the oscillations of the separation shock wave were not significant. In the subcritical mode (Figs. 6c and 7c), the oscillations of the shock wave system in front of the cowl lip, including the separation shock wave, increased considerably (see Fig. 7); in the buzz mode (Figs. 6d and 7d) (see also Supplemental Fig. S1), even the leading, conical shock from the conical nose oscillated significantly. The effects of energy deposition in the critical mode (Figs. 6b and 7b) have been previously studied in detail by Pham et al. [13]. Therefore, in this study, we focus

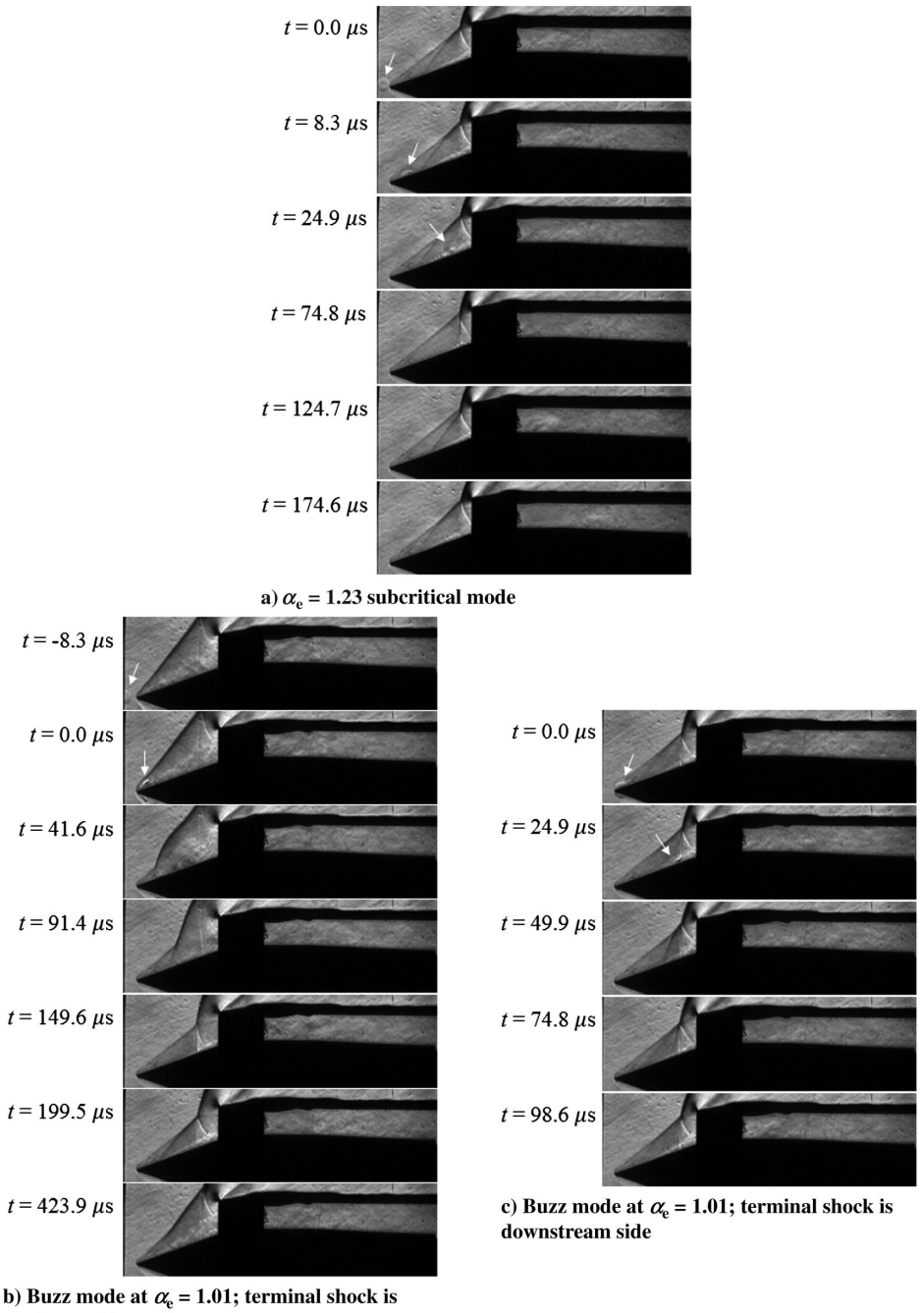

Fig. 10 Framing schlieren images of interactions between a single thermal bubble (white arrow) and shock system; t is originated at moment when the thermal bubble is formed at the leading tip of the centerbody. Video including Figs. 10b and 10c is available as Supplemental Video S2.

on the effects of energy deposition on the subcritical and buzz mode operations.

D. Flow Oscillation in Subcritical Mode

The flow characteristics in the subcritical mode, at $\alpha_e = 1.23$, are displayed in Fig. 8. As shown in Fig. 8a, the separation shock moves forward from $t = 0$ to 82.1 μs; the separation region on the compression surface, which can be recognized as the bright zone, increases accordingly. Then, from $t = 123.2$ to 164.3 μs, the separation shock moves back and the separation region decreases. An FFT analysis of the grayscale schlieren data on the dashed line in Fig. 8a is displayed in Fig. 8b. The peak spectrum of the oscillations of the conical shock is observed near $f_F = 6$ kHz. The spatial distribution of this spectrum is displayed in Fig. 8c, where the separation shock, separation region, and shock generated from the cowl lip oscillate together at $f_F = 6$ kHz. Furthermore, an oscillation spectrum of the same frequency is also observed, even inside the duct. This frequency is in the same order as the "pulsation mode." In Ref. [13], this oscillation mode was considered to be a consequence of the interaction between the boundary layer on the conical tip and the strong shock wave generated at the inlet of the duct, at a frequency from 1 to 7 kHz [21]. Although the oscillation frequency of $f_F = 6$ kHz is somewhat different from that reported in Ref. [13], the oscillation in the subcritical mode is categorized as the pulsation mode. The time histories of the internal pressure fluctuation and the FFT analysis of the pressure signals are displayed in Figs. 8d and 8e, respectively. In the subcritical mode, the oscillation of the flow was observed through visualization; however, no oscillation from the internal pressure fluctuation was observed.

E. Flow Oscillation in Buzz Mode

Figure 9 displays the characteristics of a flowfield in the buzz mode, at $\alpha_e = 1.01$. As shown in Fig. 9a, the leading conical shock moves upstream from $t = 0.65$ to 1.80 ms; and the separation region, which is recognized as a bright zone on the compression surface, expands accordingly. In this figure, the leading shock achieves its most forward position at $t = 2.39$ ms. Then, it recedes from $t = 2.39$ to 3.39 ms, causing the separation zone to also recede. In the FFT analysis of the sequential schlieren data (Fig. 9b), in front of the cowl lip, a low-frequency oscillation with $f_F \sim 0.3$ kHz is observed. The spatial distribution of this spectrum in Fig. 9c indicates that the entire conical shock oscillates at this frequency. Furthermore, as indicated in Figs. 9d and 9e, the internal pressure oscillates significantly at this frequency. Thus, unlike the subcritical mode, in the buzz mode at $\alpha_e = 1.01$, a shock wave oscillation mode is observed. The dominant frequency seems to correspond to the "Dailey buzz" [17].

The buzz frequency is typically evaluated by the following equation proposed by Newsome and based on the acoustic resonance [22]:

$$f_{B,n} = (2n+1)\frac{\hat{c}_d}{4L_d}(1 - M_d^2), \qquad n = 0, 1, 2, \ldots\ldots \tag{1}$$

However, because the average Mach number inside the duct could not be measured, this amount was replaced by a calculation, which is

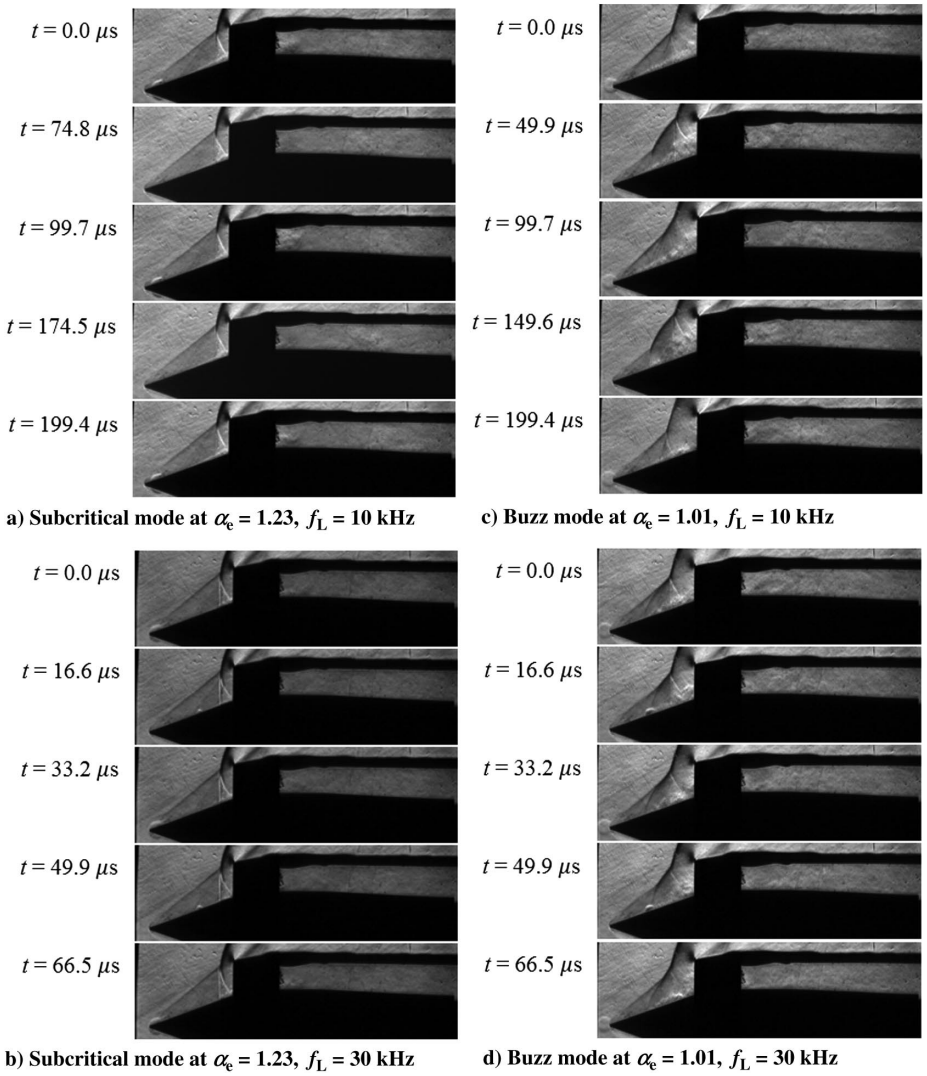

Fig. 11 Framing schlieren images of the interactions between repetitive thermal bubbles and shock system. Videos of Figs. 11c and 11d are available as Supplemental Video S3 and S4, respectively.

described as follows: The flow around the cone after the conical shock was calculated by solving the Taylor–Maccoll ordinary differential equations [23]. The Mach number of the flow after passing the conical shock was the average value of the calculation results in steps of 0.01 deg. When this flow passes through the normal shock, the flow Mach number becomes 0.69, as calculated from the normal shock relation; $\hat{c}_d$ was calculated from the obtained Mach number using the total enthalpy conservation equation. Consequently, $M_d = 0.69$, $\hat{c}_d = 319.7$ m/s, and $L_d = 0.17$ m; and the basic resonance frequency was $f_{B,0} = 0.25$ kHz. This value is close to the experimentally measured value $f_F = 0.3$ kHz. The schlieren images of Fig. 9a are observed to be well associated with the total pressure variation in the duct of Fig. 9d. Such relationships were also confirmed in another study [17]. Furthermore, the times in Figs. 9a and 9d are synchronized with each other; moreover, when the spillage mass flow is small as in Eq. (1), the internal, total pressure increases, and the leading shock begins to move upstream (see items 1 to 2 in Figs. 9a and 9d]. Accordingly, the interaction between the terminal shock and the boundary layer becomes stronger, the incoming mass flow rate decreases, and the total pressure begins to decrease. The synchronization is accompanied by a time lag due to the flow convection period on the order of 100 μs. However, at the time at item 3, the leading shock nearly achieves the maximum upstream point; it strongly interacts with the boundary layer and terminal shock at the compression surface, and the separation region increases. Thus, items 3 to 4 indicate the time when the shock exists at the maximum upstream position and the entering mass flow rate is the least; therefore, the internal pressure is also low. However, at item 4, the terminal shock begins to move backward because of the lower internal pressure; at item 6, the shock wave completes moving backward and the internal pressure increases. Therefore, items 6 to 7 are the times when the terminal shock is present downstream and the internal pressure is high. This is followed by a repetition of items 1 to 7 as the internal pressure increases with the increase in the entering mass flow rate. Thus, as described previously, buzz occurs due to the self-excited oscillation of the shock wave generated when an inconsistency occurs between the entering and exit mass flow rates.

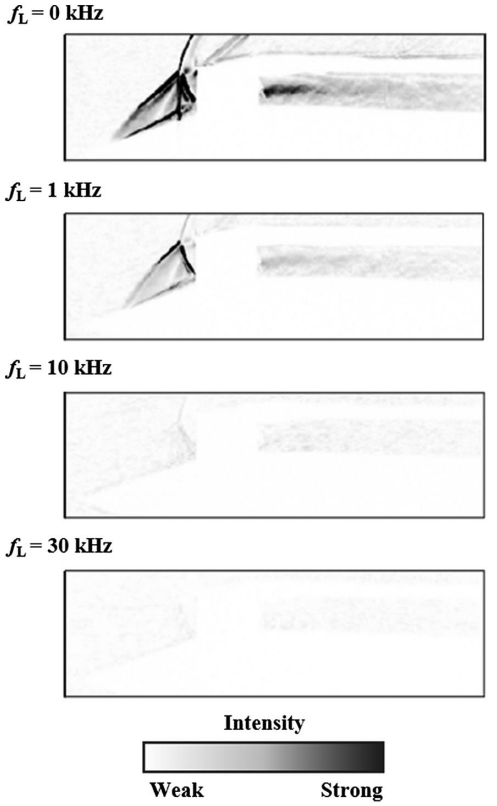

Fig. 12 Spectral density distribution at natural peak frequency of 6.0 ± 0.03 kHz of pulsation mode at different f_L values; subcritical mode at $\alpha_e = 1.23$.

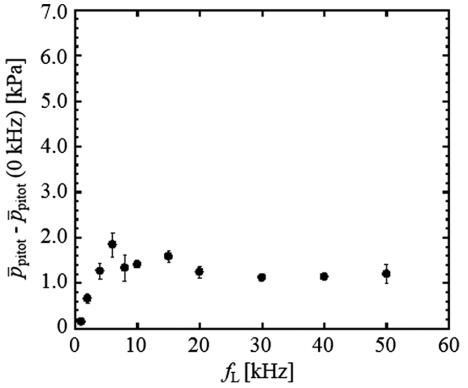

Fig. 13 Pitot pressure increment vs f_L at $\alpha_e = 1.23$: subcritical mode.

V. Effect of Single-Pulse Energy Deposition

In this section, the effects of single-energy pulse deposition on the supersonic intake performance in the subcritical and buzz modes are investigated. In the work of Iwakawa et al. [24], the experimental and numerical results were compared, and the results showed that the conversion efficiency from the laser pulse energy to the effective energy input to the bubble was approximately 40%; furthermore, assuming a calorically perfect gas and an effective volume of the laser energy absorption, the static temperature in the bubble was approximately 400 K. The interactions in the subcritical mode are displayed in Fig. 10a. The interaction pattern is observed to be similar to that in Fig. 10a at $t = 0.0$ μs; at $t = 8.3$ μs, the thermal bubble arrives at the foot of the separation shock, leading to the commencement of the SWBLI; at $t = 24.9$ μs, the separated boundary layer and associated separation shock are observed to be swept out; and at $t = 74.8$ μs, the sweeping event is complete. Then, the SWBLI pattern begins to get restored (from $t = 124.7$ to 174.6 μs). The effect of flow separation suppression by a thermal bubble was also observed in previous studies [12,13] and was termed as the "sweeping effect"; the same effect has been reproduced in this study.

The interactions between the shock system and a single thermal bubble in the buzz mode are displayed in Fig. 10b and Supplemental Fig. S2. In this mode, the effects of the bubble depend on the phase of the shock system. When the cowl shock is most upstream, the flow separation at the compression surface significantly increases, as observed in Fig. 10b, at $t = -8.3$ μs; the flowfield was significantly altered by the sweeping effect produced by the single-energy pulse, as observed in the images up to $t = 149.6$ μs. The mechanisms of the sweeping effect can be explained as a solution of a Riemann problem of a shock wave and a thermal bubble interaction [25]. When a shock wave interacts with a medium having a low acoustic impedance, expansion waves are generated behind the shock wave, thereby lowering the static pressure. As the acoustic impedance of the thermal

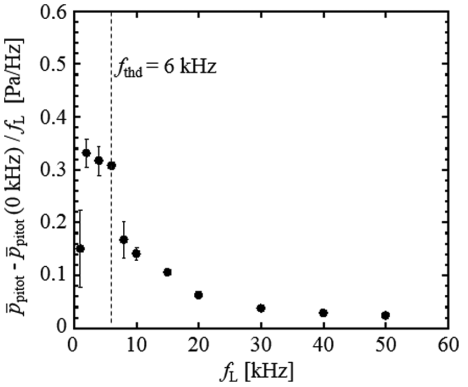

Fig. 14 Pitot pressure increment per pulse vs f_L at $\alpha_e = 1.23$: subcritical mode.

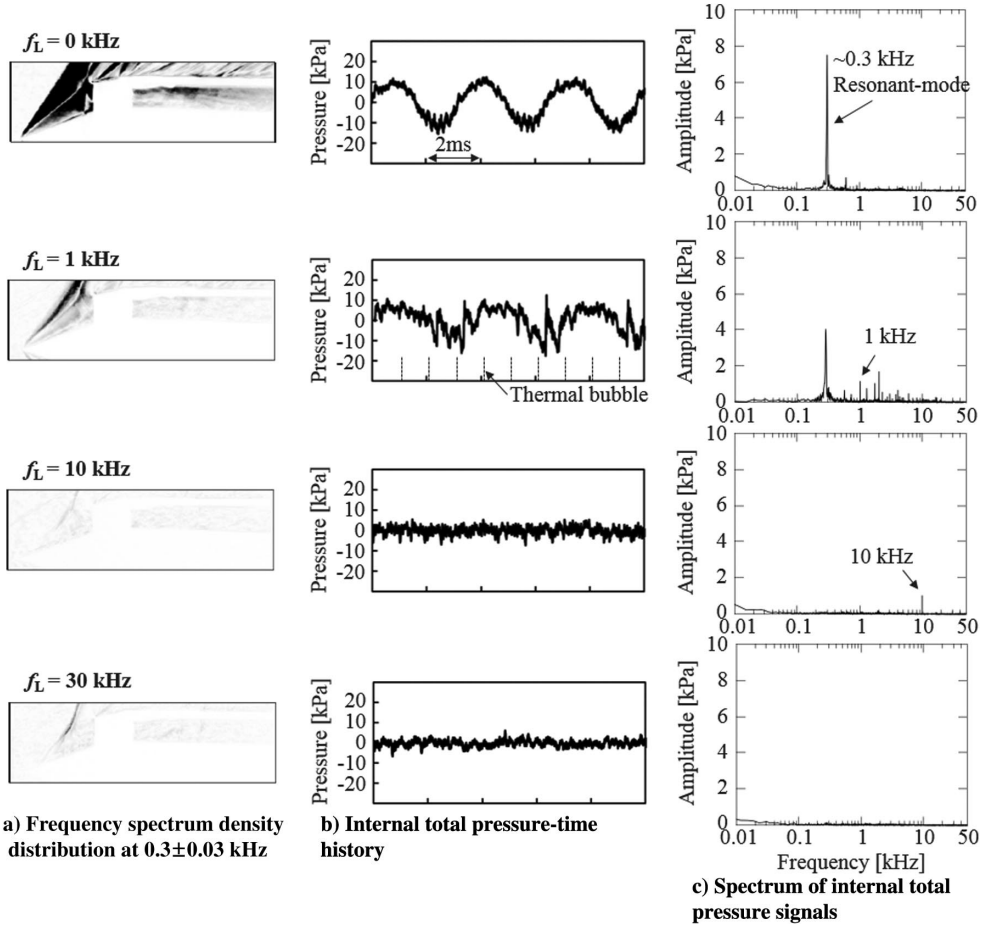

Fig. 15 Stabilization effect of repetitive energy deposition at $\alpha_e = 1.01$: buzz mode.

bubble is lower than that of the surroundings ($\rho a \propto \sqrt{p\rho} \propto \sqrt{\rho}$, where p is constant) the cowl shock is weakened after the thermal bubble enters the shock system. Moreover, because the expansion waves alleviate the adverse pressure gradient, the flow separation is also suppressed; and δ is decreased. In this case, the restoration time is considerably longer than that in the subcritical mode; it requires 423.9 μs for the shock system to restore to its original pattern. Conversely, when the cowl shock remains primarily downstream (see Fig. 10c and Supplemental Fig. S2), the flow separation region is relatively smaller. As with the terminal shock downstream, the sweeping effect on the flowfield is not significant; and the restoration time is less than 100 μs.

VI. Effect of Repetitive Energy Deposition

Figure 11 displays the sequential schlieren images with repetitive energy pulse deposition at $f_L = 10$ and 30 kHz in the subcritical and buzz modes. As displayed in Fig. 11a, the separated boundary layer and associated separation shock were swept out at $t = 74.8$ μs. Then, the state of the flowfield is restored to its original state; however, before the complete restoration, the next thermal bubble arrives and the interaction begins: At $f_L = 30$ kHz (Fig. 11b), intermittent fluctuations in the flowfield are not observed and the flowfield is steady. A similar result is observed in the case of the buzz mode at $f_L = 10$ kHz (see Fig. 11c and Supplemental Fig. S3): the separation area is temporarily suppressed. Then, at $f_L = 30$ kHz (see Fig. 11d and Supplemental Fig. S4), the periodic change at the flowfield is not observed. Furthermore, the effect of repetitive energy deposition was investigated using an FFT analysis of the visualization data and pressure measurement.

Figure 12 displays a comparison of the spectral density distribution of the natural shock oscillation frequency for different energy deposition repetition frequencies. As mentioned in Sec. IV.D, without energy deposition, a pulsation mode oscillation of 6 kHz is observed around the cowl entrance. This oscillation is marginally suppressed by the repetitive energy deposition at $f_L = 1$ kHz, and then it is almost completely suppressed at $f_L = 10$ and 30 kHz. As indicated in Fig. 13, the pitot pressure in the duct increases linearly with f_L until 6 kHz because the sweeping effect of each thermal bubble acts independently [13]. Moreover, the sweeping effect reduces the flow spillage because the separation and associated pressure loss are suppressed. However, a further increase in f_L weakens the sweeping effect because the cowl shock remains weak even after the next thermal bubble is formed. Consequently, the pressure increment decreases marginally and is saturated with increasing f_L.

The duration of the sweeping effect is important in determining the increase in pitot pressure with f_L. In this study, the duration of the sweeping effect was evaluated as the period after which the flowfield was restored to the state before the formation of the thermal bubble in the framing schlieren images. At $\alpha_e = 1.23$ in the subcritical mode, as indicated in Fig. 10a, the sweeping effect continues for 166.3 μs,

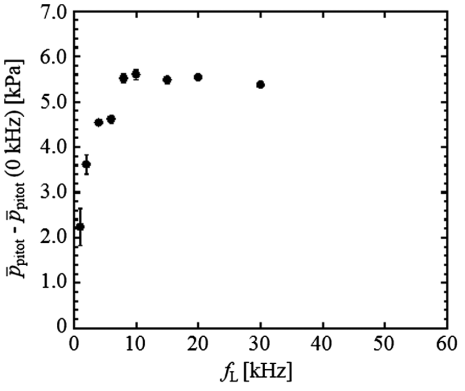

Fig. 16 Pitot pressure increment vs f_L at $\alpha_e = 1.01$: buzz mode.

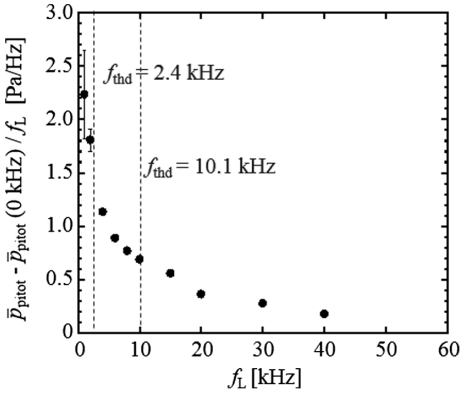

Fig. 17 Pitot pressure increment per pulse vs f_L at $\alpha_e = 1.01$: buzz mode.

thereby corresponding to the threshold frequency $f_{L,\mathrm{thd}}$ of 6 kHz against the linear effectiveness on the pitot pressure increase. As can be observed in Fig. 14, the effect on each pulse is independent in $f_L < f_{L,\mathrm{thd}}$; and the pressure increase per pulse is constant. Conversely, at $f_L > f_{L,\mathrm{thd}}$, the next thermal bubble arrives before the separation shock is restored to its original state; hence, the interaction between the separation shock and the thermal bubble weakens and the pressure increase per pulse decreases. Similar results were obtained in the research by Pham et al. [13].

Figure 15 displays the flow characteristics in the buzz mode ($\alpha_e = 1.01$) at different f_L. Even in the buzz mode, the oscillation of the shock system is observed to be suppressed by repetitive energy deposition, particularly at $f_L = 10$ kHz and higher. Furthermore, even at $f_L = 1$ kHz (Fig. 15b), the oscillation of the pitot pressure in the duct is influenced by the repetitive energy deposition. The broken lines in Fig. 15b represent the time when a thermal bubble arrives at the tip of the conical nose of the centerbody. If the thermal bubble arrives when the pressure is low or the cowl shock is upstream, the pitot pressure is increased by its arrival. As previously described, this is caused by the receding motion of the cowl shock, which leads to the suppression of the flow spillage. Conversely, if the thermal bubble arrives when the pressure is high and the cowl shock is downstream, no significant effect is observed on the internal pitot pressure signal. At $f_L = 10$ and 30 kHz, the low-frequency oscillation is observed to be almost completely suppressed. The FFT result of the pressure signal is displayed in Fig. 15c. When $f_L = 1$ kHz, the amplitude of the oscillation with 1 kHz is reduced to less than half of that with 0.3 kHz; whereas at $f_L = 10$ kHz, it is virtually unseen, and hence the oscillation spectrum of only f_L can be seen. With $f_L = 30$ kHz, all oscillation spectra are suppressed, even of f_L. As reported by Tamba et al. [19], when f_L is increased past a threshold value, interactions and even connections occur between successive bubbles; hence, the oscillation of f_L is also suppressed.

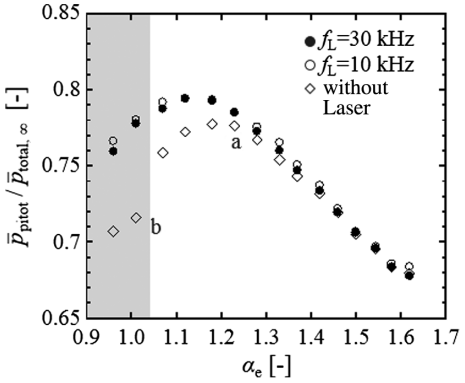

Fig. 18 Pressure recovery vs α_e with and without repetitive energy deposition; the run-to-run uncertainty in time-averaged value is less than 0.2%.

Figures 16 and 17 show that, in the buzz mode, there is a significant effect of the increase in frequency on the internal pressure. Furthermore, the threshold frequency is different from that in the subcritical mode. At $\alpha_e = 1.01$ in the buzz mode, the duration of the sweeping effect depends on the position of the terminal shock, and the two $f_{L,\mathrm{thd}}$ values for the cases where the terminal shock is the most upstream and downstream are $f_{L,\mathrm{thd}} = 2.4$ and 10.1 kHz, respectively. The lower threshold frequency $f_{L,\mathrm{thd}}$, which corresponds to the condition when the terminal shock is most upstream, is important; and the pressure increment per pulse decreases significantly as f_L increases beyond 2.4 kHz.

The effect of repetitive energy deposition on pressure recovery is summarized in Fig. 18: Although its effect is not significant in the supercritical to critical modes, the pressure recovery is significantly increased in the subcritical and buzz modes; in the buzz mode, an even larger pressure recovery is achieved. Moreover, the difference in the pitot pressure increment between $f_L = 10$ and 30 kHz is minimal. Considering these results, it can be confirmed that buzz is suppressed by the repetitive energy deposition, thereby widening the stable operation regime in the subcritical mode.

VII. Conclusions

Using a supersonic intake model, the effect of repetitive energy deposition on the supersonic intake in the subcritical and buzz modes was systematically investigated in this study; the flow instabilities were suppressed, and pressure recovery was increased by repetitive energy deposition. The occurrence of buzz was delayed, and the stable operation area was expanded by the process. In the subcritical mode, the duration of the sweeping effect was approximately 160 μs, regardless of the arrival timing of the thermal bubble. However, in the buzz mode, it depended on the arrival timing, and it was in the range of 100–420 μs. The relationship between the pressure increase amount and the frequency of the repetitive energy deposition was determined by the threshold value $f_{L,\mathrm{thd}}$, which in turn was determined by the duration of the sweeping effect. When $f_L < f_{L,\mathrm{thd}}$, the pressure increase amount was proportional to the frequency and the effect per pulse was constant; when $f_L > f_{L,\mathrm{thd}}$, the effect per single pulse decreased: $f_{L,\mathrm{thd}} = 6$ kHz in the subcritical mode, and $f_{L,\mathrm{thd}} = 2.4$ kHz in the buzz mode.

Acknowledgments

This research was supported by the Japan Society for Promotion of Science Grant-in-Aid for Scientific Research (A) no. 18H03813. The authors would like to thank A. Saito and Y. Adachi, of the Technical Division at Nagoya University, for their valuable technical assistance.

References

[1] Babinsky, H., and Harvey, K. J., *Shock Wave-Boundary-Layer Interactions*, Cambridge Aerospace Series, Cambridge Univ. Press, New York, 2011.

[2] Obery, L. J., and Cubbison, R. W., "Effectiveness of Boundary-Layer Removal Near Throat of Ramp-Type Side Inlet at Free-Stream Mach Number of 2.0," NACA RM E54I14, 1954.

[3] Trapier, S., Duveau, P., and Deck, S., "Experimental Study of Supersonic Inlet Buzz," *AIAA Journal*, Vol. 44, No. 10, 2006, pp. 2354–2365. https://doi.org/10.2514/1.20451

[4] Soltani, M. R., Younsi, J. S., and Farahani, M., "Effects of Boundary-Layer Bleed Parameters on Supersonic Intake Performance," *Journal of Propulsion and Power*, Vol. 31, No. 3, 2015, pp. 826–836 https://doi.org/10.2514/1.B35461

[5] Dolling, S. D., "Fifty Years of Shock-Wave/Boundary-Layer Interaction Research: What Next?" *AIAA Journal*, Vol. 39, No. 8, 2001, pp. 1517–1531. https://doi.org/10.2514/2.1476

[6] Knight, D., "Survey of Aerodynamic Drag Reduction at High Speed ByEnergy Deposition," *Journal of Propulsion and Power*, Vol. 24, No. 6, 2008, pp. 1153–1167. https://doi.org/10.2514/1.24595

[7] Leonov, S., Yarantsev, D., and Falepin, F., "Flow Control in a Supersonic Inlet Model by Electrical Discharge," *Journal of Progress in Flight Physics*, Vol. 3, Jan. 2012, pp. 557–568. https://doi.org/10.1051/eucass/201203557

[8] Falepin, F., Firsov, A. A., Yarantsev, D., Goldfeld, A. M., Timofeev, K., and Leonov, S., "Plasma Control of Shock Wave Configuration in Off-Design Mode of M = 2 Inlet," *Journal of Experiment in Fluids*, Vol. 56, No. 3, 2015, https://doi.org/10.1007/s00348-015-1928-4

[9] Narayanaswamy, V., Raja, L. L., and Clemens, N. T., "Control of a Shock/Boundary-Layer Interaction by Using a Pulsed-Plasma Jet Actuator," *AIAA Journal*, Vol. 50, No. 1, 2012, pp. 246–249. https://doi.org/10.2514/1.J051246

[10] Narayanaswamy, V., Raja, L. L., and Clemens, N. T., "Control of Unsteadiness of a Shock Wave/Turbulent Boundary Layer Interaction by Using a Pulsed-Plasma-Jet Actuator," *Physics of Fluids*, Vol. 24, No. 7, 2012, Paper 76101. https://doi.org/10.1063/1.4731292

[11] Osuka, T., Erdem, E., Hasegawa, N., Majima, R., Tamba, T., Yokota, S., Sasoh, A., and Kontis, K., "Laser Energy Deposition Effectiveness on Shock-Wave Boundary-Layer Interactions over Cylinder-Flare Combinations," *Physics of Fluids*, Vol. 26, No. 9, 2014, Paper 096103. https://doi.org/10.1063/1.4896288

[12] Pham, H. S., Shoda, T., Tamba, T., Iwakawa, A., and Sasoh, A., "Impacts of Laser Energy Deposition on Flow Instability over Double-Cone Model," *AIAA Journal*, Vol. 55, No. 9, 2017, pp. 2992–3000. https://doi.org/10.2514/1.J055670

[13] Pham, H. M., Myokan, T., Tamba, T., Iwakawa, A., and Sasoh, A., "Effects of Repetitive Laser Energy Deposition on Supersonic Duct Flows," *AIAA Journal*, Vol. 56, No. 2, 2018, pp. 542–553. https://doi.org/10.2514/1.J056190

[14] Ferri, A., and Nucci, L. M., "The Origin of Aerodynamic Instability of Supersonic Inlets at Subcritical Conditions," NACA RM L50 K30, 1951.

[15] Dailey, C. L., "Supersonic Diffuser Instability," Ph.D. Dissertation, California Inst. of Technology, Pasadena, CA, 1954.

[16] Fisher, S. A., Neale, M. C., and Brooks, A. J., "On the Sub-Critical Stability of Variable Ramp Intakes at Mach Numbers Around 2," National Gas Turbine Establishment, Rept. ARC-R/M-3711, London, England, Feb. 1970.

[17] Lee, H. J., Lee, B. J., Kim, S. D., and Jeung, I. S., "Flow Characteristics of Small-Sized Supersonic Inlets," *Journal of Propulsion and Power*, Vol. 27, No. 2, 2011, pp. 306–318. https://doi.org/10.2514/1.46101

[18] Kim, J. H., Matsuda, A., Sakai, T., and Sasoh, A., "Wave Drag Reduction with Acting Spike Induced by Laser-Pulse Energy Depositions," *AIAA Journal*, Vol. 49, No. 9, 2011, pp. 2076–2078. https://doi.org/10.2514/1.J051145

[19] Tamba, T., Pham, H. S., Shoda, T., Iwakawa, A., and Sasoh, A., "Frequency Modulation in Shock Wave-Boundary Layer Interaction by Repetitive-Pulse Laser Energy Deposition," *Physics of Fluids*, Vol. 27, No. 9, 2015, Paper 091704. https://doi.org/10.1063/1.4931924

[20] Iwakawa, A., Shoda, T., Pham, H. S., Tamba, T., and Sasoh, A., "Suppression of Low-Frequency Shock Oscillations over Boundary Layer by Repetitive Laser Pulse Energy Deposition," *Aerospace*, Vol. 3, No. 2, 2016, p. 13, Paper 13. https://doi.org/10.3390/aerospace3020013

[21] Feszty, D., Badcock, K. J., and Richards, B. E., "Driving Mechanisms of High-Speed Unsteady Spiked Body Flows, Part 1: Pulsation Mode," *AIAA Journal*, Vol. 42, No. 1, 2004, pp. 95–106. https://doi.org/10.2514/1.9034

[22] Newsome, R. W., "Numerical Simulation of Near-Critical and Unsteady, Subcritical Inlet Flow," *AIAA Journal*, Vol. 22, No. 10, 1984, pp. 1375–1379. https://doi.org/10.2514/3.48577

[23] Taylor, G. I., and Maccoll, J. W., "The Air Pressure on a Cone Moving at High Speeds. I," *Proceedings of the Royal Society of London, Series A: Mathematical and Physical Sciences*, Vol. 139, No. 838, 1933, pp. 278–297. https://doi.org/10.1098/rspa.1933.0017

[24] Iwakawa, A., Sakai, T., and Sasoh, A., "Repetition Frequency Dependence of Wave Drag Reduction Induced by Laser-Pulse-Energy Depositions," *Transactions of the Japan Society for Aeronautical and Space Sciences*, Vol. 11, Jan. 2013, pp. 53–60.

[25] Iwakawa, A., Shoda, T., Majima, R., Pham, H. S., and Sasoh, A., "T Mach Number Effect on Supersonic Drag Reduction Using Repetitive Laser Energy Depositions over a Blunt Body," *Transactions of the Japan Society for Aeronautical and Space Sciences*, Vol. 60, No. 5, 2017, pp. 303–311. https://doi.org/10.2322/tjsass.60.303

D. S. Stewart
Associate Editor